

Article

Analysis of Soil Slope Stability under Underground Coal Seam Mining Using Improved Radial Movement Optimization with Lévy Flight

Haotian Li, Liangxing Jin *  and Pingting Liu

Department of Civil Engineering, Central South University, Changsha 410075, China; 224811062@csu.edu.cn (H.L.); liupt1997@163.com (P.L.)

* Correspondence: jlx871162@csu.edu.cn

Abstract: Underground coal seam mining significantly reduces the stability of slopes, especially soil slopes, and an accurate evaluation of the stability of soil slopes under underground mining conditions is crucial for mining safety. In this study, the impact of coal seam mining is considered as the additional horizontal and vertical stresses acting on the slope, and an equation for calculating the safety factor of soil slopes under underground mining conditions is derived based on the rigorous Janbu method. Then, the Improved Radial Movement Optimization (IRMO) algorithm is introduced and combined with Lévy flight optimization to conduct global optimization searches, obtaining the critical sliding surface and corresponding safety factor of the soil slope under underground coal seam mining. Through comparisons with the numerical simulation results in three different case studies, the feasibility of applying the IRMO algorithm with Lévy flight to analyze the stability of soil slopes under underground mining is demonstrated. This ensures the accuracy and stability of the calculation results while maintaining a high convergence efficiency. Furthermore, the effects of the mining thickness and mining direction on slope stability are analyzed, and the results indicate that a smaller mining thickness and mining along the slope are advantageous for slope stability. The method proposed in this study provides valuable insights for preventing the slope instability hazards caused by underground coal seam mining.

Keywords: improved radial movement optimization (IRMO) algorithm; Lévy flight; underground coal seam mining; slope stability

MSC: 68T20; 74L10



Citation: Li, H.; Jin, L.; Liu, P. Analysis of Soil Slope Stability under Underground Coal Seam Mining Using Improved Radial Movement Optimization with Lévy Flight. *Mathematics* **2024**, *12*, 1566. <https://doi.org/10.3390/math12101566>

Academic Editor: Ivan Lorenčin

Received: 22 April 2024

Revised: 10 May 2024

Accepted: 16 May 2024

Published: 17 May 2024



Copyright: © 2024 by the authors. Licensee MDPI, Basel, Switzerland. This article is an open access article distributed under the terms and conditions of the Creative Commons Attribution (CC BY) license (<https://creativecommons.org/licenses/by/4.0/>).

1. Introduction

China is a country with abundant coal resources, but there is very little coal suitable for open-pit mining. A large amount of coal resources are deeply buried beneath mountains and existing slopes [1,2]. Therefore, underground mining has become a new trend in coal resource development. However, when mining coal seams under soil slopes, the goaf formed by mining changes the original stress equilibrium state of the slope, leading to phenomena such as slope collapse and landslides in mining areas [3,4]. These unstable slopes not only pose a serious threat to the lives of residents but also damage farmland vegetation, exacerbating soil erosion and desertification [5,6].

Therefore, conducting in-depth research on the stability of soil slopes under underground coal seam mining is of great significance. In terms of the deformation and failure mechanisms of soil slopes under underground mining, scholars have conducted research using similar model tests and numerical simulations. Wang et al. [7], through similar simulation tests, summarized that the deformation evolution of slopes under underground coal mining has three stages: surface modification, structural modification, and time-dependent deformation. Ding et al. [8] and Shi et al. [9], focusing on the Anjialing coal mine, established a FLAC3D numerical analysis

model and a similar test model to investigate the mechanical behavior of overlying strata and the deformation process of slopes during coal mining, respectively.

In addition to clarifying the deformation and failure mechanisms, a quantitative assessment of the stability of slopes under underground coal seam mining is also essential. The slope safety factor is an essential metric for assessing the stability of slopes. Scholars have studied the computation and solution of the safety factor using the finite element and limit equilibrium methods for slopes subjected to underground mining in great detail [10,11]. Leng et al. [12], based on the Hoek–Brown strength criterion, calculated the safety factor of karst slopes in Pusa after underground mining using FLAC3D, and obtained the changes in the stability of the karst slope after mining. Zhang et al. [13], using FLAC3D, calculated the variation in the slope safety factor caused by different mining conditions and determined that the influence level of the goaf on slope stability is related to its scale and relative position to the slope. Xu et al. [14], based on the mechanism of bedding plane landslides induced by underground coal mining and the characteristics of mining-induced landslides, analyzed the influence of mining on slopes from the perspective of changes in the sliding surface morphology. They derived a calculation formula for the safety factor of slopes considering mining effects based on the limit equilibrium theory. Shi et al. [15] combined the ant colony and genetic algorithms to search for the sliding surface of slopes jointly. They used the vector sum method, considering the stress field of slopes, to solve the safety factor of slopes under mining conditions. Zhang et al. [16] studied the influence of the depth/thickness ratio on slope stability using the limit equilibrium method, based on an analysis of the surface movements induced by underground coal mining and additional stresses on the slope.

The key to using the limit equilibrium method to calculate the safety factor of soil slopes under underground coal seam mining is to find the critical sliding surface corresponding to the minimum safety factor from multiple potential sliding surfaces. Scholars have used various optimization algorithms such as genetic algorithms [17,18], ant colony algorithms [15,19], and particle swarm algorithms [20,21] to address this issue and have achieved good results. As a new type of metaheuristic optimization algorithm, the IRMO algorithm has a high convergence speed and excellent global search capabilities. It has been widely applied in the field of slope stability analysis [22–24] and foundation bearing capacity analysis [25], and has gained widespread recognition. Although the IRMO algorithm has good performance compared to other algorithms, there is still the problem of not being able to escape the local extremum when solving complex high-dimensional nonlinear problems. Lévy flight is a type of random walk with a heavy-tailed distribution of step length [26], and can be combined with the IRMO algorithm to avoid getting stuck in local optima and improve the accuracy of the calculation results.

This study conducted a stability analysis of soil slopes under underground coal seam mining using the IRMO algorithm with Lévy flight. Based on the rigorous Janbu method, the additional horizontal and vertical stresses caused by mining were considered in force and moment equilibrium, leading to the derivation of the calculation equation for the safety factor of soil slopes under underground coal seam mining. This equation was then set as the fitness function for the IRMO algorithm with Lévy flight to locate the critical sliding surface and its corresponding minimum safety factor. The feasibility of the proposed method is demonstrated through three different case studies, and the influence of different coal seam mining thicknesses and mining directions on slope stability is studied.

2. Analysis of Soil Slope Stability under Underground Coal Seam Mining

2.1. Sliding Surface Model of Slopes under Underground Coal Seam Mining

Underground coal seam mining causes deformation that results in the production of vertical cracks at the top of the slope, which significantly affects the shape of the sliding surface of the slope. The lower limit of the depth h of these cracks can be calculated according to Equation (1), and the upper limit does not exceed half of the slope height [27]. By considering the influence of vertical cracks and combining this with the non-circular sliding surface construction method proposed by Zolfaghari [18], the sliding surface model

of slopes under underground mining can be established, as shown in Figure 1. The expression and constraints of the sliding surface are shown in Equation (2).

$$h = \frac{2c}{\gamma} \tan(45^\circ + \frac{\varphi}{2}) \tag{1}$$

where c is the cohesion of the soil, φ is the internal friction angle of the soil, and γ is the volumetric weight of the soil.

$$\left. \begin{aligned} & [x, h, \alpha_1, \Delta\alpha_2, \Delta\alpha_3, \dots, \Delta\alpha_n] \\ & x_{\min} < x < x_{\max} \\ & h_{\min} < h < h_{\max} \\ & 10^\circ < \alpha_1 < 70^\circ \\ & 0^\circ < \Delta\alpha_i < 30^\circ \end{aligned} \right\} \tag{2}$$

where x is the starting position of the sliding surface, typically taken as $x_{\min} = 0$, and x_{\max} is taken as half of the length of the slope model; h is the depth of the vertical crack, where h_{\min} is calculated according to Equation (1), and h_{\max} is taken as half of the slope height; α_1 is the angle between the bottom surface of the first block and the vertical direction; and $\Delta\alpha_i$ is the incremental angle of the subsequent block relative to the previous one.

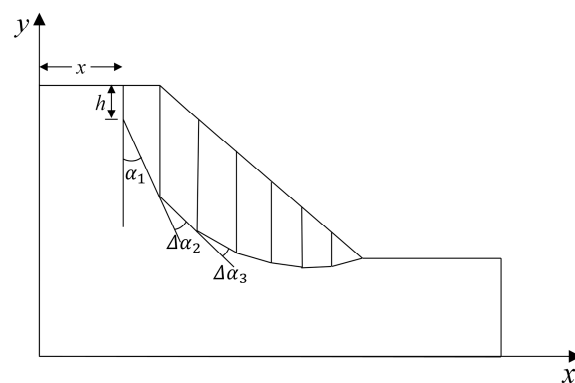


Figure 1. Sliding surface model of slopes under underground mining.

2.2. Calculation of Slope Safety Factor under Underground Coal Seam Mining

2.2.1. Additional Stress Caused by Underground Mining

Unlike slopes under common conditions, the goaf formed by underground mining results in slopes with two free faces: the foot of the slope and the goaf, subjecting the slope to the effects of mining subsidence and slope sliding simultaneously. Therefore, in addition to its weight, the slope also experiences additional horizontal stress F_a and vertical stress F_b due to surface horizontal deformation, inclination, and subsidence. The specific calculation formulas are as follows [16,28,29]:

$$F_a = P_m C_i W_i \tag{3}$$

$$F_b = \eta_i W_i + \eta_i c l \tag{4}$$

$$P_m = \frac{M \cdot D}{H \cdot F} \tan \beta_s \tag{5}$$

$$C_i = \lambda(\varepsilon_i + \varepsilon'_i) + \xi(i_i + i'_i) \tag{6}$$

$$\eta_i = (P_m \cdot w_i) / (H - H_S) \tag{7}$$

where P_m is the mining influence coefficient. C_i is the coefficient for calculating additional horizontal stress. W_i is the weight of the i -th slice. η_i is the coefficient for calculating additional vertical stress. M is the mining thickness. H is the mean mining depth under the slope. D is the mining width. F is the lithological coefficient, which can be selected according to Table 1. β_s is the slope angle. i_i and i'_i are, respectively, the static and dynamic

inclination deformation of the top edge of the i -th slice; when the direction of inclination deformation is the same as the inclination of the slope, take a positive value, and when it is opposite, take a negative value. ε_i and ε_i' are, respectively, the static and dynamic horizontal deformation of the top edge of the i -th slice, ε_i is positive for extension and negative for compression, and ε_i' is always positive and its value is about 60% of ε_i ; this is only considered when ε_i is negative and the slice is located above the goaf area. λ is the lateral pressure coefficient, $\lambda = \mu / (1 - \mu)$. μ is Poisson's ratio. ω_i is the subsidence of the top edge of the i -th slice. $\zeta = H_S / H$, H_S is the height of the slope.

Table 1. Lithological coefficient.

Name of Rock and Earth Mass	F	Name of Rock and Earth Mass	F
Slope deposits and silty sand	1.0~1.2	Sandy shale (calcareous cementation)	1.8~2.0
Silty clay and clay	1.2~1.4	Medium hard sandstone and limestone	2.0~2.2
Mudstone and siltstone	1.4~1.6	Hard sandstone and limestone	2.2~2.5
Sandy mudstone and muddy shale	1.6~1.8	Extremely hard limestone and quartz sandstone	2.8~3.0

2.2.2. Calculation Method Based on Janbu Method

The Janbu method, as a type of limit equilibrium method, simultaneously considers both force equilibrium and moment equilibrium. It is applicable to slip surfaces of any shape and exhibits high accuracy. Therefore, this paper adopts the Janbu method, considering the additional horizontal stress and additional vertical stress, to derive the calculation formula for the slope safety factor under underground mining. As shown in Figure 2, a Janbu method slice mechanical analysis model of slopes under underground mining is established. In the model, E_i and E_{i+1} are the normal forces between slices. T_i and T_{i+1} are the tangential forces between slices. W_i is the weight of the i -th slice. F_a is the additional horizontal stress induced by underground mining on the i -th slice. F_b is the additional vertical stress induced by underground mining on the i -th slice. N_i is the normal force on the bottom of the i -th slice. S_i is the tangential force on the bottom of the i -th slice. α_i is the angle between the bottom of the i -th slice and the horizontal direction. Δx_i is the width of the i -th slice. y_i and y_{i+1} are the heights of tangential forces. p_i is the vertical distance from the centroid of the slice to the center O_i of the sliding surface. l_i is the bottom length of the i -th slice.

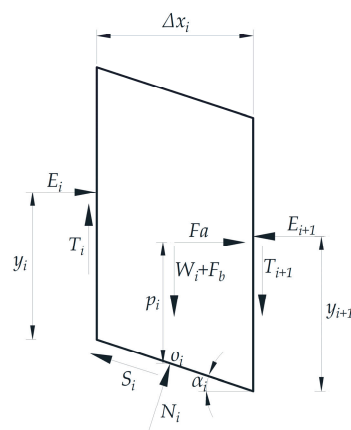


Figure 2. Mechanical analysis model of slice i .

The specific derivation process is as follows:
 From $\sum F_x = 0$, the following can be derived:

$$\Delta E_i = E_{i+1} - E_i = N_i \sin \alpha_i - S_i \cos \alpha_i + F_a \tag{8}$$

From $\sum F_y = 0$, the following can be derived:

$$N_i \cos \alpha_i = T_{i+1} - T_i + W_i + F_b - S_i \sin \alpha_i = \Delta T_i + W_i + F_b - S_i \sin \alpha_i \tag{9}$$

Therefore:

$$\Delta E_i = -S_i \left(\cos \alpha_i + \frac{\sin^2 \alpha_i}{\cos \alpha_i} \right) + (\Delta T_i + W_i + F_b) \tan \alpha_i + F_a \tag{10}$$

For the entire slice, there is $\sum \Delta E_i = 0$:

$$\sum \Delta E_i = -\sum S_i \left(\cos \alpha_i + \frac{\sin^2 \alpha_i}{\cos \alpha_i} \right) + \sum (\Delta T_i + W_i + F_b) \tan \alpha_i + F_a = 0 \tag{11}$$

Take the moment for point O_i , from $\sum M = 0$, the following can be derived:

$$(T_i + T_{i+1}) \frac{\Delta x_i}{2} + E_i \left(y_i + \frac{\Delta x_i}{2} \tan \alpha_i \right) + F_a p_i = E_{i+1} \left(y_{i+1} - \frac{\Delta x_i}{2} \tan \alpha_i \right) \tag{12}$$

Equation (12) can be simplified as follows:

$$\frac{(T_i + T_{i+1})}{2} + E_i \left(\frac{\tan \alpha_i}{2} + \frac{y_i}{\Delta x_i} \right) + F_a \frac{p_i}{\Delta x_i} = E_{i+1} \left(\frac{y_{i+1}}{\Delta x_i} - \frac{\tan \alpha_i}{2} \right) \tag{13}$$

Substituting $T_{i+1} = T_i + \Delta T_i$ into Equation (13) and neglecting higher-order terms, the following can be derived:

$$T_i = (E_i + \Delta E_i) \left(\frac{y_{i+1}}{\Delta x_i} - \frac{\tan \alpha_i}{2} \right) - E_i \left(\frac{y_i}{\Delta x_i} + \frac{\tan \alpha_i}{2} \right) - F_a \frac{p_i}{\Delta x_i} \tag{14}$$

According to the theory of shear strength, the limit equilibrium condition at the sliding surface is as follows:

$$S_i = \frac{\tau_i l_i}{F_S} = \frac{c_i l_i}{F_S} + N_i \frac{\tan \varphi}{F_S} \tag{15}$$

where $l_i = \Delta x_i / \cos \alpha_i$; by solving Equations (9) and (15) simultaneously, the following can be concluded:

$$S_i = \frac{(\Delta T_i + W_i + F_b) \tan \varphi + c_i \Delta x_i}{\sin \alpha_i \tan \varphi + F_S \cos \alpha_i} \tag{16}$$

Substituting Equation (16) into Equation (11), the following can be derived:

$$F_S = \frac{\sum \left\{ c_i l_i \cos \alpha_i + (\Delta T_i + W_i + F_b) \tan \varphi \right\} \frac{\sec^2 \alpha_i}{1 + \frac{\tan \varphi \tan \alpha_i}{F_S}}}{\sum (\Delta T_i + W_i + F_b) \tan \alpha_i + F_a} \tag{17}$$

Equation (17) is an implicit function for F_S , which needs to be solved by an iterative method. The specific process is as follows:

1. Initially assume $\Delta T_i = 0$, in which case Equation (17) only has F_S as an unknown quantity.
2. Use the Newton–Raphson iteration method to solve Equation (17), obtaining the first safety factor F_{S1} .
3. Substitute F_S and ΔT_i into Equation (16) to calculate S_i for each slice. Then, substitute S_i into Equation (10) to obtain ΔE_i for each slice. Substitute E_i and ΔE_i into Equation (14) to obtain T_i and ΔT_i .
4. Substitute the newly obtained ΔT_i into Equation (17) to obtain a new safety factor F_{Si} .
5. Repeat steps 3 and 4 until $F_{Si} - F_{Si-1} < \delta$, where δ is the accuracy of a preset safety factor, typically set to $\delta = 0.005$. The final obtained F_S is the safety factor of slopes under underground mining.

3. Improved Radial Movement Optimization

3.1. Concepts of IRMO

Rahmani and Yusof [30] proposed the Radial Movement Optimization (RMO) algorithm in 2014. This algorithm is characterized by its simplicity, small storage space requirement, rapid convergence, and resistance to premature convergence. However, when applying this algorithm to calculate the slope safety factor and search for a critical sliding

surface, it was found that the computed results failed to converge to the same sliding surface, indicating instability. To address this issue, Pan et al. [24] improved the data structure based on the RMO algorithm and proposed the IRMO algorithm. By considering the self-feedback capability of particles, the IRMO algorithm enhances the accuracy and stability of search results.

3.1.1. The Working Principle of IRMO

(1) Generate the initial particle group

Within the algorithm, define a matrix $[X]$ of size $nop \times nod$ to store the position information of nop particles in a nod -dimensional space. Randomly generate the initial particle position X_i according to Equations (18) and (19), and the range of values for each particle in the j -th dimension is $[\min x_j, \max x_j] (1 \leq j \leq nod)$. Calculate and compare the fitness function value $f(X_i)$ of the initial particle group ($1 \leq i \leq nop$) and select the particle with the minimum fitness function value in the initial particle group as the initial center position $Center^1$. And set this position as the current global best position $Gbest^1$.

$$x_{i,j} = \min x_j + rand(0, 1)(\max x_j - \min x_j) \tag{18}$$

$$X_i = [x_{i,1} \quad x_{i,2} \quad \cdots \quad x_{i,nod}] \tag{19}$$

(2) Generate a new generation of the particle group

Considering the self-feedback capability of particles, generate the position of the new generation of the particle group according to Equations (20) and (21). Then, calculate the fitness function value $f(X_i^k)$ of the new generation of each particle X_i . Update the best position $Rbest^k$ of this generation with the minimum value between the fitness function values of the new and previous generation. If $Rbest^k$ is superior to the global best position $Gbest^k$, update $Gbest^k$ as well.

$$x_{i,j}^k = \begin{cases} Center_j^k + rand(-0.5, 0.5) \cdot (\max x_j - \min x_j) \cdot W^k, & p < \frac{W^k}{2} \\ x_{i,j}^{k-1}, & p \geq \frac{W^k}{2} \end{cases} \tag{20}$$

$$W^k = 1 - \frac{k}{G}, p = rand(0, 1) \tag{21}$$

where k is the current number of iterations.

(3) Update central position

The new center position is influenced by both the best position of this generation $Rbest^k$ and the global best position $Gbest^k$, which can be calculated using Equation (22). In this equation, $C1$ and $C2$ are scaling factors affecting the convergence speed and computational accuracy. Their values range from 0.4 to 0.9 [30]. In this study, we take $C1 = 0.4$ and $C2 = 0.5$.

$$Center^{k+1} = Center^k + C1(Gbest^k - Center^k) + C2(Rbest^k - Center^k) \tag{22}$$

(4) Algorithm stop condition

If k has not reached the maximum number of iterations G , return to step (2) to continue the calculation until the condition is met. At this point, the global best position $Gbest^k$ represents the optimal optimization path, and the fitness function value of the best position is the desired extremum of the multidimensional function.

3.1.2. The Particle Position Update Strategy Based on Lévy Flight

The IRMO algorithm sometimes encounters the issue of getting trapped in local optima when generating new-generation particle positions. Lévy flight is a random walk process with step lengths following a heavy-tailed distribution. Its movement pattern, characterized by frequent short steps interspersed with occasional long steps, enables it to escape local optima and exhibits good global search capabilities [31]. By utilizing Lévy flight for optimization when generating new generations of particles, the algorithm can meet the requirements for convergence accuracy while also having a certain probability of generating larger step lengths, thereby escaping local optima and achieving the global optimum.

The step length S of Lévy flight can be calculated using the Mantegna method [32]:

$$S = \frac{u}{|v|^{1/\beta}} \tag{23}$$

where u and v are random numbers drawn from normal distributions, and u follows $N(0, \sigma^2)$ and v follows $N(0, 1)$, with $\beta = 1.5$.

σ can be calculated using Equation (24):

$$\sigma = \left(\frac{\Gamma(1 + \beta) \sin(\frac{\pi\beta}{2})}{\beta\Gamma(\frac{1+\beta}{2}) \times 2^{(\frac{\beta-1}{2})}} \right)^{\frac{1}{\beta}} \tag{24}$$

Therefore, the equation for updating the positions of new generations of particles in the IRMO algorithm can be represented by Equation (25):

$$x_{i,j}^k = \begin{cases} Center_j^k + rand(-0.5, 0.5) \cdot (\max x_j - \min x_j) \cdot W^k, & p < \frac{W^k}{2} \\ Cx_{i,j}^{k-1} + \lambda Gbest^k + 0.01(Gbest^k - x_{i,j}^{k-1})S, & p \geq \frac{W^k}{2} \end{cases} \tag{25}$$

where $C = 2 \times rand(0, 1) \times (1 - \frac{k}{G})$, $\lambda = e^{\frac{1-G}{G+1-k}}$.

The flowchart of the IRMO algorithm with Lévy flight is shown in Figure 3.

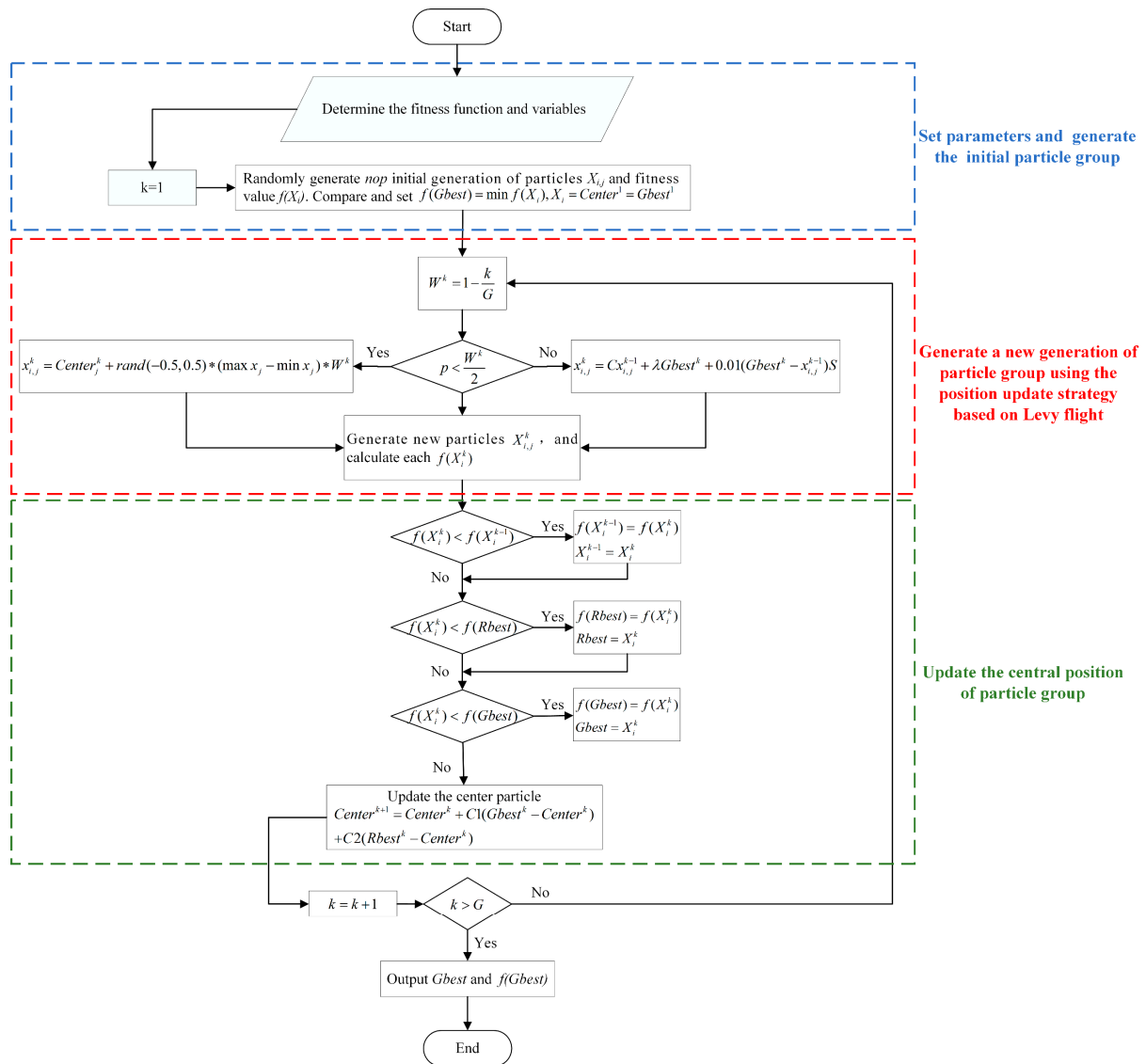


Figure 3. The flowchart of the IRMO algorithm with Lévy flight.

3.1.3. Simulation Case Analysis

To verify the superiority of the IRMO algorithm with Lévy flight, testing is conducted using the Sphere function and Rastrigin function. The Sphere function is a unimodal benchmark function with a unique global minimum value of 0, while the Rastrigin function is a multimodal benchmark function with multiple local extrema and a global minimum value of 0, as is shown in Table 2.

Table 2. Benchmark functions.

Name	Expression	Dimension	Range
Sphere	$f(x) = \sum_{i=1}^n x_i^2$	30	$x_i \in [-100, 100]$
Rastrigin	$f(x) = \sum_{i=1}^n (x_i^2 - 10 \cos(2\pi x_i) + 10)$	30	$x_i \in [-5.12, 5.12]$

The number of particles (*nop*) is set as 50. The maximum iteration number (*G*) is 1000. The Sphere function and Rastrigin function are each tested 20 times using the IRMO algorithm with Lévy flight and without Lévy flight.

Table 3 shows that the IRMO algorithm with Lévy flight achieves higher precision in the search results. Although it requires slightly more search time, the trade-off is acceptable. Lévy flight sacrifices a relatively small amount of computational efficiency for higher computational accuracy, resulting in a superior search performance for the IRMO algorithm.

Table 3. Results of benchmark functions.

Function	The IRMO Algorithm without Lévy Flight		The IRMO Algorithm with Lévy Flight	
	Mean Value	Mean Search Time	Mean Value	Mean Search Time
Sphere	5.7479×10^{-8}	0.1655	3.9515×10^{-175}	0.2729
Rastrigin	6.1×10^{-3}	0.1778	1.4588×10^{-8}	0.2912

3.2. Implementation of IRMO

In the IRMO algorithm, the nod-dimensional vectors representing particle positions can correspond to the variable set $[x, h, \alpha_1, \Delta\alpha_2, \Delta\alpha_3, \dots, \Delta\alpha_n]$ for constructing the sliding surfaces of slope under underground mining. Thus, using *nop* particles to represent *nop* sliding surfaces, a matrix can be constructed, as shown in Equation (26):

$$X_{i,j} = \begin{bmatrix} x_{1,1} & h_{1,2} & \alpha_{1,3} & \Delta\alpha_{1,4} & \cdots & \Delta\alpha_{1,nod} \\ x_{2,1} & h_{2,2} & \alpha_{2,3} & \Delta\alpha_{2,4} & \cdots & \Delta\alpha_{2,nod} \\ \vdots & \vdots & \vdots & \vdots & \ddots & \vdots \\ x_{nop,1} & h_{nop,2} & \alpha_{nop,3} & \Delta\alpha_{nop,4} & \cdots & \Delta\alpha_{nop,nod} \end{bmatrix} \quad (26)$$

After constructing the sliding surface of slopes under underground mining and dividing it into slices, the calculation equation for the safety factor of slope under underground coal seam mining (Equation (17)) is used as the fitness function of the IRMO algorithm with Lévy flight. Subsequently, the algorithm is used to calculate and compare the safety factors of each sliding surface. The movement of particles in the solution space is manifested as the movement of sliding surfaces in the slope model. Ultimately, the sliding surface with the minimum safety factor represents the critical sliding surface of the slope.

According to the above theory, a program for analyzing the stability of soil slopes under underground coal seam mining based on the IRMO algorithm with Lévy flight has been developed using QT Creator 4.12.2. In practical use, the user needs to input parameters such as the soil material properties of the slope (cohesion *c*, internal friction angle φ , volumetric weight γ), coal mining conditions (mining thickness *M*, mining depth *H*, mining width *D*, lithology factor *F*), the subsidence and deformation of the slope (slope

subsidence ω , inclination deformation i and horizontal deformation ε), and the parameters of the IRMO algorithm (the number of particles nop , particles dimension nod , and maximum iteration count G).

In the process of slope stability analysis, the correct selection of parameters such as the soil material properties of the slope, coal mining conditions, and the subsidence and deformation of the slope is crucial, as this determines the accuracy of the analysis results. Therefore, the complexity of geological conditions and the errors in the surface displacement monitoring system are issues that cannot be ignored. For the selection of soil and rock material parameters, multiple samples should be taken within the mining area and the average of the laboratory test results should be used. The selection of parameters for coal seam mining conditions should be determined based on the distribution, the properties of coal seams, and the actual mining situation in the mining area. For the selection of parameters for the subsidence and deformation of the slope, the surface displacement monitoring results and FLAC3D numerical simulation results can be comprehensively considered to ensure the rationality of parameter selection.

The specific workflow for the stability analysis of soil slopes under underground coal seam mining based on the IRMO algorithm with Lévy flight is illustrated in Figure 4.

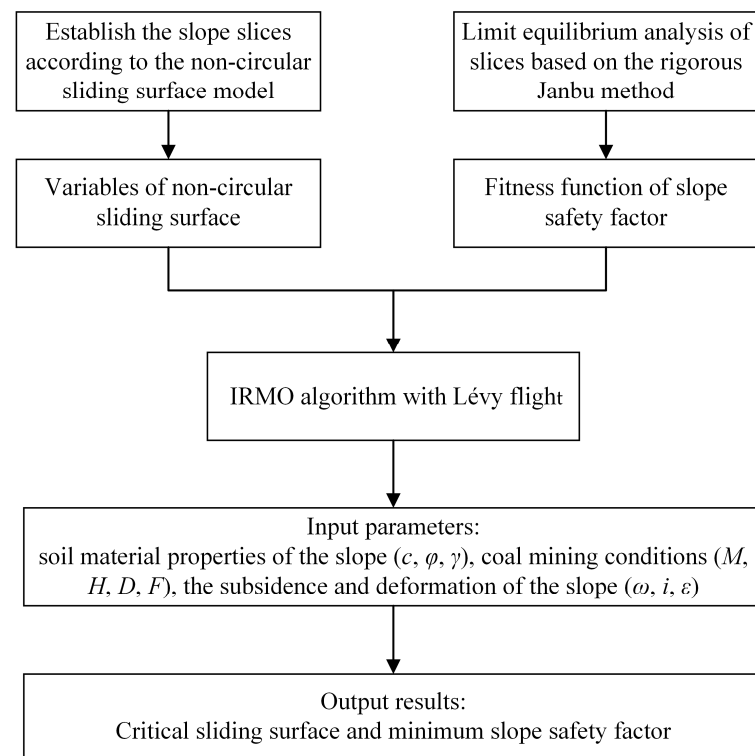


Figure 4. The flowchart of the stability analysis of soil slopes under underground coal seam mining.

4. Case Studies

To validate the feasibility of the stability analysis of soil slopes under underground coal seam mining based on the IRMO algorithm with Lévy flight in this study, the following cases will be analyzed and verified.

4.1. Case Study 1: Slope under Full Mining

Case study 1 refers to the literature of Zhao et al. [33]. The slope in this case is located in the Ningtiaota coal mine in northern Shaanxi, China. The predominant soil strata composition in this area is loess, while the rock strata mainly consist of sandstone. Figure 5 shows the model of the slope under underground coal mining in case study 1, and the material parameters of each rock and soil strata are listed in Table 4.

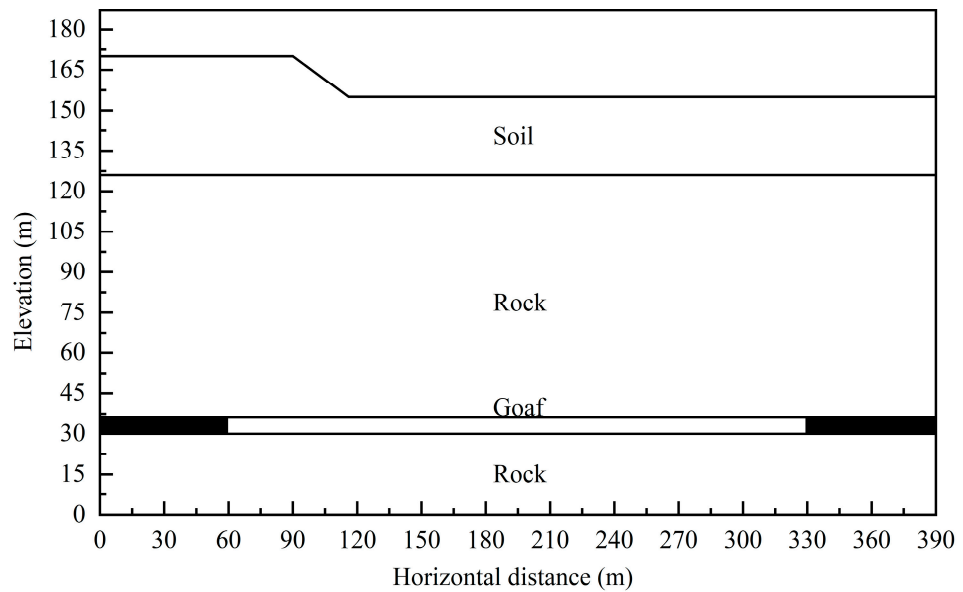


Figure 5. Slope model of case study 1.

Table 4. Material parameters of case study 1.

Lithology	Cohesion c /(kPa)	Internal Friction Angle ϕ /(°)	Volumetric Weight γ /(kN/m ³)	Poisson’s Ratio μ	Elastic Modulus E /(GPa)	Tensile Strength σ_t /(MPa)
Soil strata	6.95	27.5	17.4	0.25	0.12	0.02
Rock strata	4750	38	23.8	0.3	9.3	2.5
Coal	1620	22	13.3	0.38	2.1	0.5

Referring to the literature [33], the overlying rock strata thickness above the coal seam in the model is 90 m. To ensure full mining, the mining width D of the coal seam is set to 1.5 times the mining depth H . Additionally, the ratio of the overlying rock strata thickness to soil strata thickness J_Z and the ratio of the rock strata thickness to mining thickness J_C are used as influencing parameters to categorize different mining conditions. The IRMO algorithm with Lévy flight is used to calculate the slope safety factor under different underground mining conditions, and compared with the results calculated by FLAC3D in case study 1; the calculation results are listed in Table 5.

Table 5. Underground mining conditions and calculation results.

Mining Conditions		Mining Influence Coefficient P_m	F_S of Case Study 1 [33]	F_S of This Study
J_Z	J_C			
1	30	1.0825	1.1615	1.1426
1	45	0.7216	1.2467	1.2022
2	30	1.0825	1.1832	1.1983
2	45	0.7216	1.2579	1.2398
3	30	1.0825	1.1946	1.2264
3	45	0.7216	1.2637	1.2572
4	30	1.0825	1.2022	1.2367
4	45	0.7216	1.2687	1.2663
Unexcavated		—	1.3370	1.3412

Figure 6 shows the variation curve of the slope safety factor under different mining conditions. It can be observed that the safety factor obtained from both studies exhibits the same trend, increasing with the increase of J_Z . Moreover, the slope safety factor calculated using the IRMO algorithm with Lévy flight is very close to the results in the literature [33],

with a maximum difference of only 0.0445, which is within an acceptable range. This indicates that the calculation results of the method proposed in this study are highly accurate.

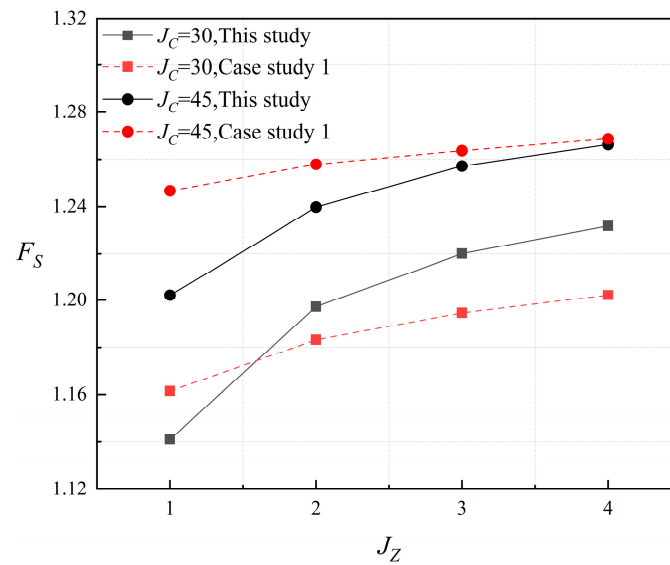


Figure 6. Slope safety factor under different mining conditions.

In addition to the accuracy of the calculation results, stability is also an important indicator used to measure the feasibility of the algorithm. The IRMO algorithm with Lévy flight and the RMO algorithm were utilized to perform 20 searches for four excavation conditions, with J_c set to 30, and J_z set to 1, 2, 3, and 4, respectively. The results of the slope safety factor and critical sliding surfaces obtained from 20 consecutive runs are shown in Figures 7 and 8, respectively.

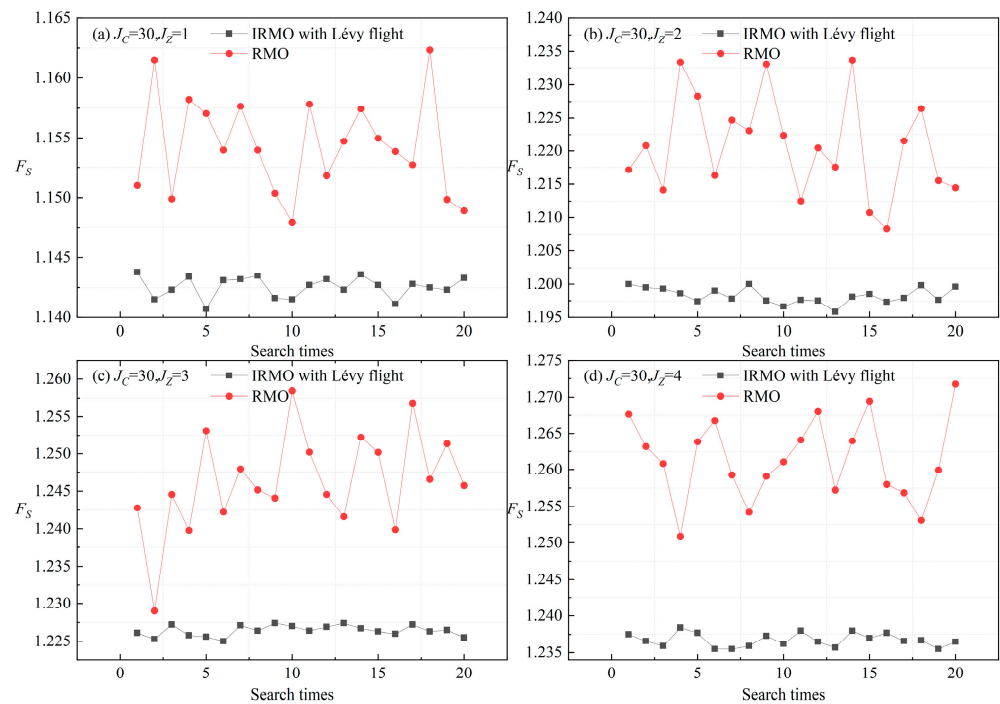


Figure 7. Search results of the slope safety factor.

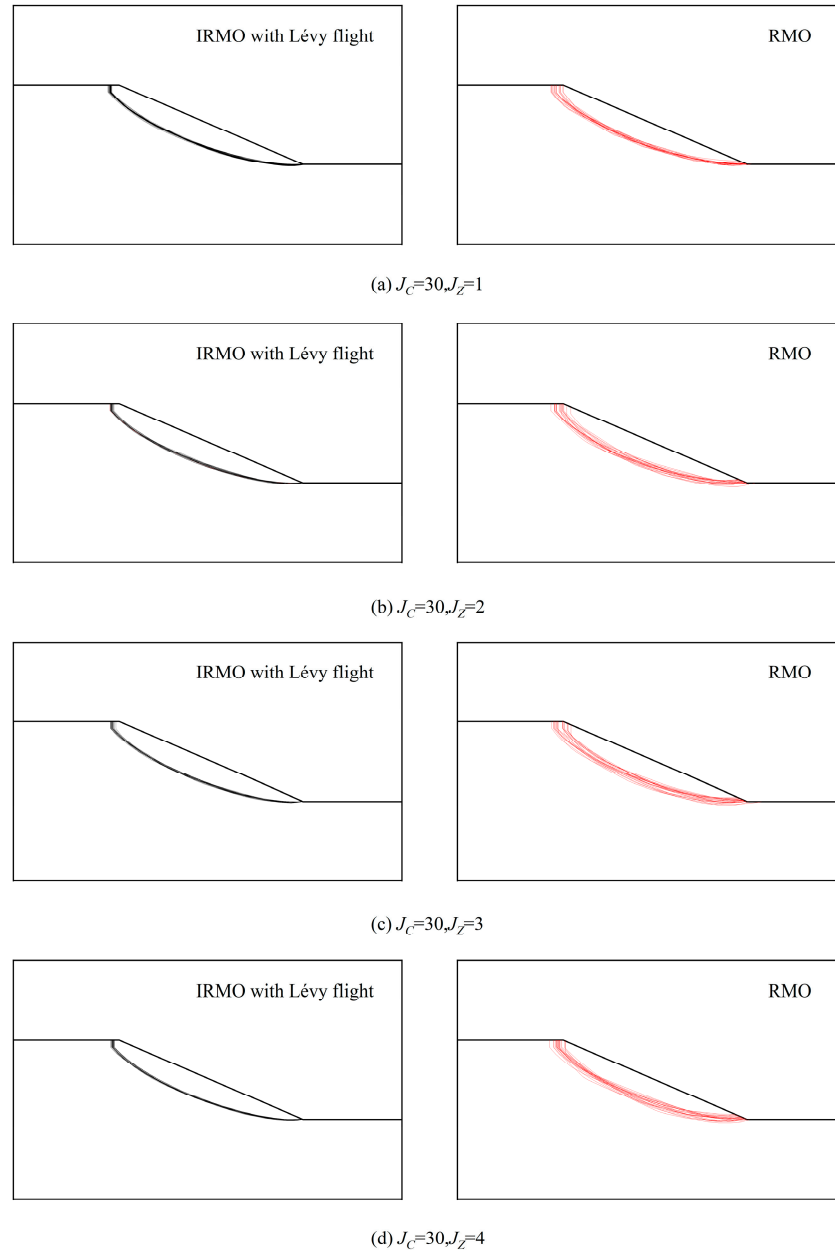


Figure 8. Search results of the critical sliding surfaces of the slope.

From Figure 7 and Table 6, it can be observed that compared to the RMO algorithm, the slope safety factor calculated using the IRMO algorithm with Lévy flight for 20 consecutive runs under different mining conditions has smaller average values and standard deviations, with a maximum standard deviation of only 0.0012. These results for the IRMO algorithm with Lévy flight show a better performance regarding stability.

Table 6. Comparison of stability between IRMO with Lévy flight and RMO after 20 runs.

Mining Condition	The IRMO Algorithm with Lévy Flight		The RMO Algorithm	
	Average F_S	Standard Deviation	Average F_S	Standard Deviation
$J_C = 30, J_Z = 1$	1.1426	0.0008	1.1543	0.0041
$J_C = 30, J_Z = 2$	1.1983	0.0012	1.2207	0.0075
$J_C = 30, J_Z = 3$	1.2264	0.0007	1.2363	0.0067
$J_C = 30, J_Z = 4$	1.2367	0.0009	1.2615	0.0056

In Figure 8, the black line represents the critical sliding surfaces obtained using the IRMO algorithm with Lévy flight, while the red line represents the critical sliding surfaces obtained using the RMO algorithm. Figure 8 reveals that compared to the RMO algorithm, the critical sliding surfaces obtained from 20 consecutive runs using the IRMO algorithm with Lévy flight under the four different mining conditions all have higher overlaps and smaller fluctuation ranges. These results from Figures 7 and 8 demonstrate the high stability of the IRMO algorithm with Lévy flight when applied to calculating the slope safety factor and searching for the critical sliding surfaces of slopes under underground mining.

Figure 9 shows the convergence of the slope safety factor with the number of iterations under different mining conditions using the IRMO algorithm with Lévy flight and the RMO algorithm, respectively. It can be observed that compared to the RMO algorithm, the IRMO algorithm with Lévy flight has a faster convergence speed, and that the safety factor of all four mining conditions reaches stability before the 45th iteration. This indicates that the IRMO algorithm with Lévy flight possesses the advantages of a fast convergence and high computational efficiency.

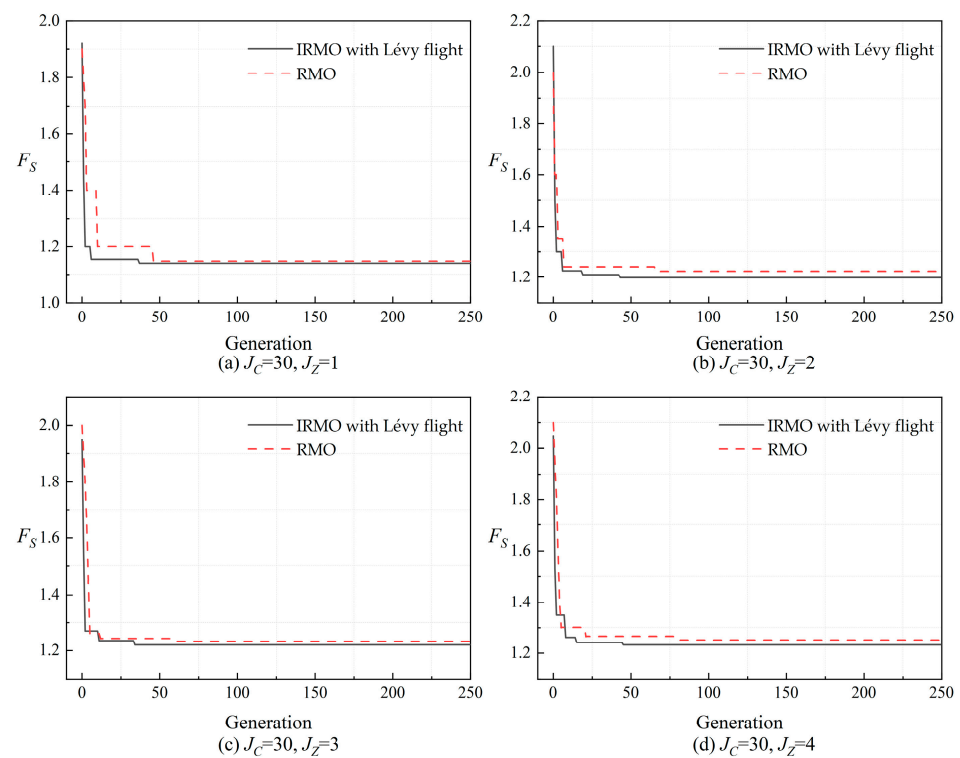


Figure 9. The comparison of the convergence efficiency of algorithms under different mining conditions.

Figure 10 illustrates the variation in the critical sliding surfaces of the slope constructed by the IRMO algorithm with Lévy flight, with J_c set to 30, and J_z set to 1, 2, 3, and 4, respectively. As the soil thickness increases, the starting point of the critical sliding surface moves further away from the slope crest, and the area of the critical sliding surface increases, indicating that the slope is more disturbed by the goaf.

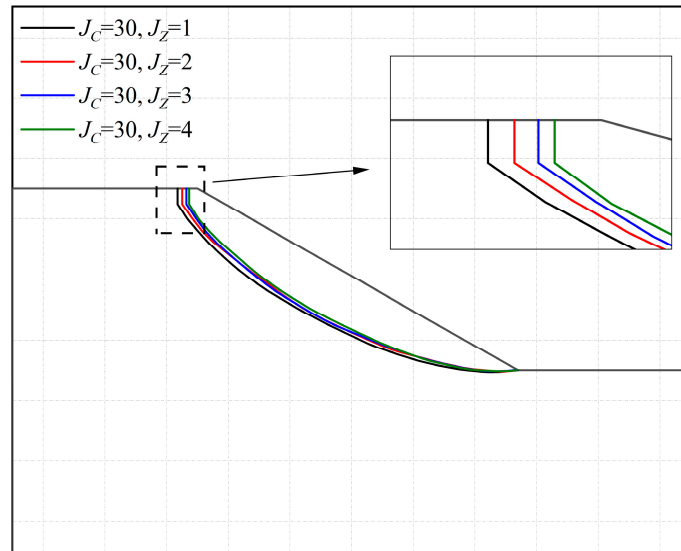


Figure 10. The critical sliding surface of the slope under different mining conditions.

4.2. Case Study 2: Slope under Stepwise Mining

In reference to the case study by Ren Peng [34], the feasibility of applying the IRMO algorithm with Lévy flight to the stability analysis of slope under underground mining is further validated by comparing it with the results from FLAC3D. The studied slope in case study 2 is located in the Antaibao coal mine in Shuozhou, China. The region is characterized by loess hilly terrain, with a thick layer of clay covering the surface. The specific model of the slope is depicted in Figure 11, and the material parameters of the slope’s rock and soil strata are listed in Table 7.

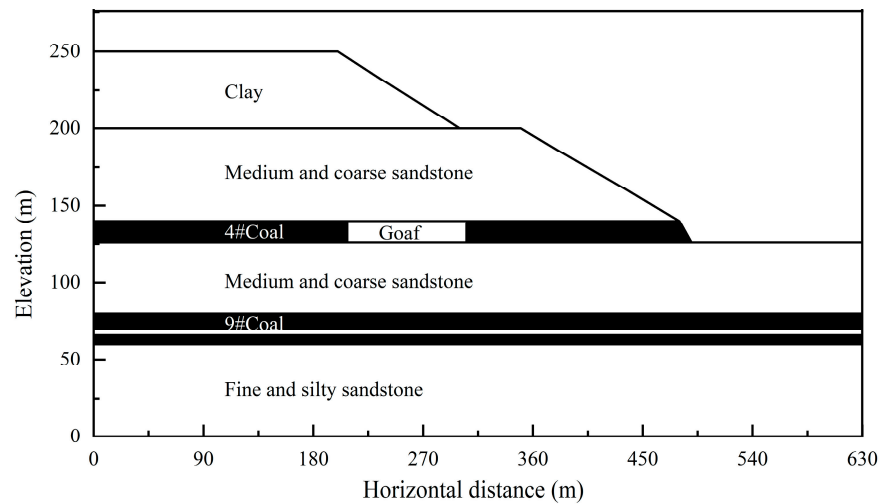


Figure 11. Slope model of case study 2.

Table 7. Material parameters of case study 2.

Lithology	Cohesion c /(kPa)	Internal Friction Angle ϕ /(°)	Volumetric Weight γ /(kN/m ³)	Poisson’s Ratio μ	Elastic Modulus E /(GPa)	Tensile Strength σ_t /(MPa)
Clay	23	27.5	19.5	0.25	0.12	0.02
Medium and Coarse sandstone	846	28	22.1	0.21	24.3	6.6
Fine and Silty sandstone	889	29	24.8	0.23	23.9	7.1
4#Coal	110	22	14.1	0.36	2.1	0.7
9#Coal	120	22	14.2	0.36	2.5	0.7

Excavation of the 4# coal seam is carried out in steps, with each step advancing 10 m. The mining thickness M is 10 m, and the mining depth H is 74 m. The safety factor of the clay slope after each step of excavation is calculated using both the IRMO algorithm with Lévy flight and FLAC3D. The specific excavation settings and calculation results are shown in Table 8.

Table 8. Stepwise excavation settings and calculation results.

Excavation Situation	The x-Coordinate of the Excavation Area (m)	Mining Width (m)	Mining Influence Coefficient P_m	F_S of FLAC3D	F_S of This Study
Unexcavated	—	—	—	1.52	1.4912
First excavation	250~260	10	0.3378	1.49	1.4823
Second excavation	250~270	20	0.6757	1.45	1.4601
Third excavation	250~280	30	1.0135	1.41	1.4222
Fourth excavation	250~290	40	1.3514	1.36	1.3679
Fifth excavation	250~300	50	1.6892	1.31	1.3013
Sixth excavation	250~310	60	2.0271	1.24	1.2211
Seventh excavation	250~320	70	2.3649	1.14	1.0621

Figure 12 shows the contour map of the maximum shear strain increment obtained from the FLAC3D simulation after stepwise excavation. The contour map of the maximum shear strain increment reflects the evolution process of internal movement paths within the slope. It can be observed that when excavation to 20 m is performed, the internal structure of the slope remains stable without significant damage. Upon excavation to 40 m, shear strain increments penetrate to the slope crest on the left side and to the slope toe on the right side of the goaf, while a potential sliding surface emerges. With further excavation to 60 m, the shear strain increment and the area of the potential sliding surface continue to increase, indicating a significant decrease in slope stability and a higher risk of landslide instability.

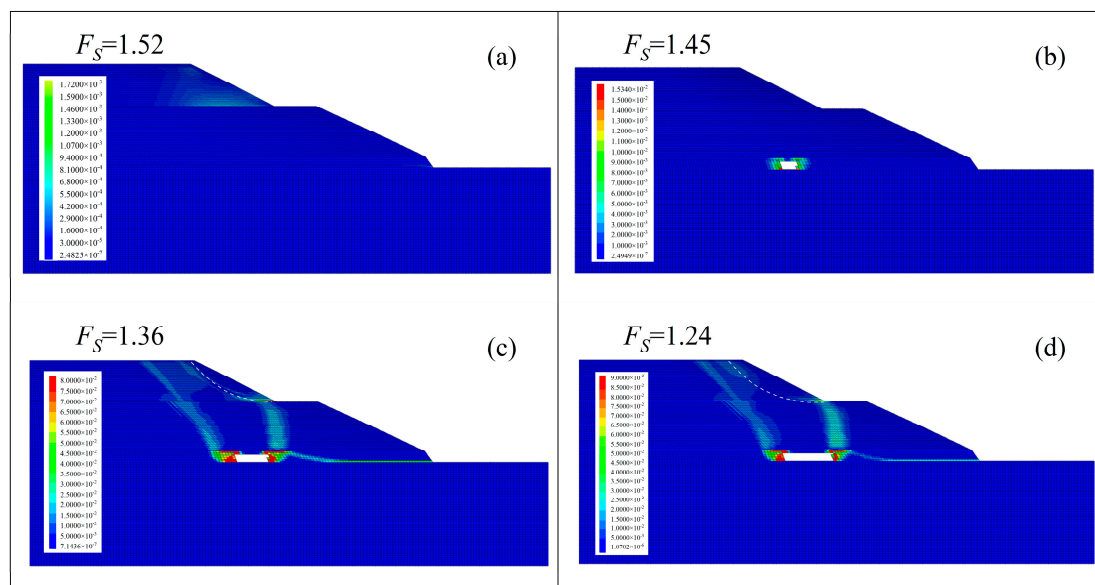


Figure 12. Contour map of maximum shear strain increment. (a) Not excavated; (b) Excavated 20 m; (c) Excavated 40 m; (d) Excavated 60 m.

To further investigate the accuracy of the IRMO algorithm with Lévy flight, the safety factor and critical sliding surface of the clay slope under underground mining conditions obtained using the IRMO algorithm with Lévy flight are compared with the results from the FLAC3D numerical simulations. The specific comparison results are shown in Figures 13 and 14, respectively.

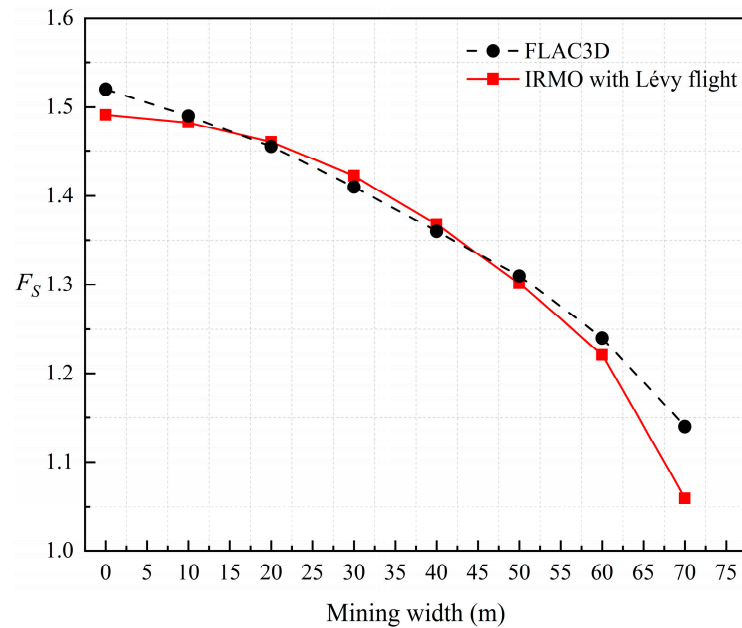


Figure 13. Comparison of slope safety factor.

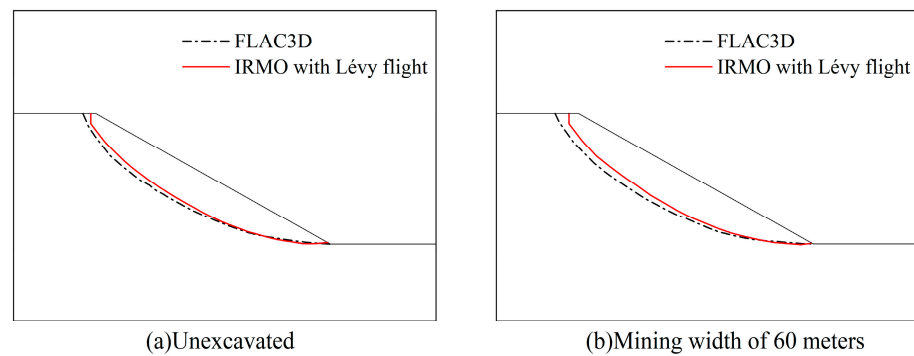


Figure 14. Comparison of the critical sliding surface.

From Figure 13, it can be observed that the safety factor of the clay slope after stepwise excavation obtained by both methods exhibits the same trend of decreasing with increasing mining width, and the rate of decrease in the slope safety factor gradually accelerates. Moreover, the safety factor obtained using the IRMO algorithm with Lévy flight is very close to that obtained using FLAC3D numerical simulation, with a maximum difference of only 7.1%. In Figure 14, the red solid line represents the critical sliding surface of the slope constructed using the IRMO algorithm with Lévy flight, while the black dashed line represents the slope sliding surface obtained by FLAC3D numerical simulation. It can be noticed that the critical sliding surfaces obtained by both methods have a high degree of overlap. Additionally, the critical sliding surface with tensile cracks constructed using the IRMO algorithm with Lévy flight is closer to the top of the slope compared to the circular sliding surface. The comparison with numerical simulation results fully demonstrates the high feasibility of using the IRMO algorithm with Lévy flight to analyze the stability of slopes under underground mining.

4.3. Case Study 3: Sliding Fissures of Slope

When the slope is located above the goaf, the coupling effect of surface fragmentation and slope movement causes the formation of sliding fissures on the slope surface, significantly reducing the stability of the slope. Reference [28] provides a predictive formula for the development of sliding fissures, as shown in Equations (27)–(29). K represents the ratio of the down-sliding force of each slice to the anti-sliding force. The maximum value of K

corresponds to the least stable slope block, resulting in local failure and the formation of sliding fissures.

$$T_i = W_i[(1 + \eta_i) \sin \alpha_i + P_m C_i \cos \alpha_i] \tag{27}$$

$$R_i = W_i \tan \varphi_i [(1 + \eta_i) \cos \alpha_i - P_m C_i \sin \alpha_i] + c_i l_i \tag{28}$$

$$K = \frac{\sum_{i=1}^n T_i}{\sum_{i=1}^n R_i} \tag{29}$$

where T_i is the down-sliding force of each slice, and R_i is the anti-sliding force of each slice.

After determining the development position of the sliding fissure in the slope under underground mining, the sliding fissure angle can be calculated according to Equation (30). As shown in Figure 15, S is the development position of the sliding fissure, z is the vertical distance from the sliding fissure to the goaf, d is the horizontal distance from the sliding fissure to the boundary of the goaf, and δ is the sliding fissure angle.

$$\delta = \arctan \frac{z}{d} \tag{30}$$

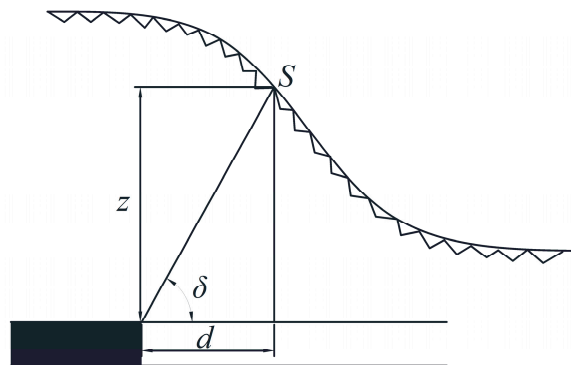


Figure 15. Profile of sliding fissure.

Referring to the case study of slope under underground coal seam mining in the literature by Liu et al. [28], the critical sliding surface of the slope was determined using the IRMO algorithm with Lévy flight, and the sliding fissure angle was calculated in this study. The slope is situated in the Daliuta coal mine of the Shendong mining area in China, and the geological structure of the area is simple, mainly composed of sandstone and fine sandstone. The main component of the slope is clay, and the properties of the slope are adopted as follows: $c = 26$ KPa, $\varphi = 24^\circ$, $\gamma = 18.9$ kN/m³, $\mu = 0.26$ [28]. The slope model and the critical sliding surface obtained by using the IRMO algorithm with Lévy flight are shown in Figure 16.

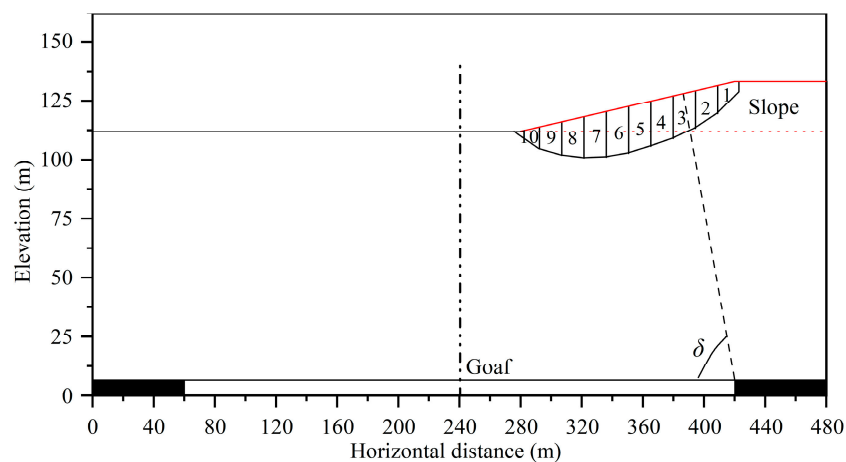


Figure 16. Slope model of case study 3.

After obtaining the division of slices on the sliding surface of the slope under underground mining, the T_i and R_i of each slice are calculated according to Equations (27) and (28). Finally, the value of K at each slice is calculated. The specific calculation results are listed in Table 9.

Table 9. Calculation results of each slice.

Slice n	$\sum_{i=1}^n T_i / (\text{kN})$	$\sum_{i=1}^n R_i / (\text{kN})$	K
1	1848.32	1101.16	1.678
2	5010.22	2728.37	1.836
3	9114.76	4714.88	1.933
4	12,977.07	7023.57	1.848
5	16,913.11	9465.49	1.787
6	20,294.02	12,057.51	1.683
7	22,845.88	14,634.72	1.561
8	24,605.19	16,985.94	1.449
9	25,456.52	18,869.64	1.349
10	25,465.75	19,927.12	1.278

From Table 9, it can be observed that the maximum value of K occurs at the third slice of the slope, indicating the most likely location for the development of the sliding fissure. From this, the sliding fissure angle is calculated to be $\delta = 74.5^\circ$. As shown in Table 10, the slope safety factor and sliding fissure angle obtained using the IRMO algorithm with Lévy flight are in good agreement with the field-measured data. This indicates that the application of the IRMO algorithm with Lévy flight for analyzing the stability of slopes under underground mining is highly feasible.

Table 10. Comparison of calculation results.

Method of Calculation	Slope Safety Factor	Sliding Fissure Angle	Error
Field measurement [28]	instability	76.4°	—
Liu's study [28]	0.816	75.3°	1.44%
This study	0.783	74.5°	2.49%

5. The Influence of Different Underground Mining Conditions on Slope Stability

The stability of soil slopes under underground coal seam mining is not only related to the geological conditions and hydrogeological conditions but also to the mining conditions, such as the mining thickness and mining direction. In this section, the IRMO algorithm with Lévy flight is used to analyze the stability of slopes under different mining conditions from the perspective of the variation in the slope safety factor.

5.1. The Influence of Mining Thickness

To verify the influence of different mining thicknesses on slope stability, the slope model from case study 2 is used. The 4 # coal seam is excavated in steps along the same direction at a thickness of 6 m, 10 m, and 14 m from the same starting position, each with a step length of 10 m. The safety factor F_S of the clay slope is calculated using the IRMO algorithm with Lévy flight after each step of excavation. Table 11 shows the parameter settings of different mining thicknesses.

Table 11. Parameter settings of mining thickness.

Mining Thickness $M/(\text{m})$	Mining Depth $H/(\text{m})$	The x-Coordinate of the Excavation Starting Position (m)	The Length of Each Step of Excavation (m)
6	74	250	10
10			
14			

According to the “Design Code for Open-pit Mine in Coal Industry” (GB50197-2015) [35], the critical safety factor for non-working bench slopes with a service life of less than 10 years should be 1.1–1.2, for a service life greater than 10 years but less than 20 years, it should be 1.2, and for a service life greater than 20 years, it should be 1.3. In case study 2, the design service life of the mining area is greater than 10 years but less than 20 years, so the critical slope safety factor chosen is 1.2.

As shown in Figure 17, when the mining thickness is 6 m, the slope safety factor F_S decreases to 1.2104 after excavating 70 m, reaching the critical safety factor; when the mining thickness is 10 m, F_S decreases to 1.2211 after excavating 60 m; and when the mining thickness is 14 m, F_S decreases to 1.2021 after excavating only 50 m, reaching the critical safety factor. It can be seen that the mining thickness has a significant impact on the stability of the slope. Under the same conditions, the smaller the mining thickness, the more stable the slope for the same mining width. From Figure 16, it can also be observed that with a constant mining thickness, F_S decreases rapidly with the increase in the mining width. When the slope is close to instability, F_S will decrease significantly. Taking a 10 m mining thickness as an example, F_S is 1.3013 at a mining width of 50 m, and 1.2211 at a mining width of 60 m, a decrease of 6.16%. If another 10 m of excavation is carried out, as the mining width is 70 m, the slope safety factor F_S is only 1.06, a decrease of 13.19%. Thus, when the slope safety factor reaches the critical safety factor, excavation should be stopped immediately to avoid accidents.

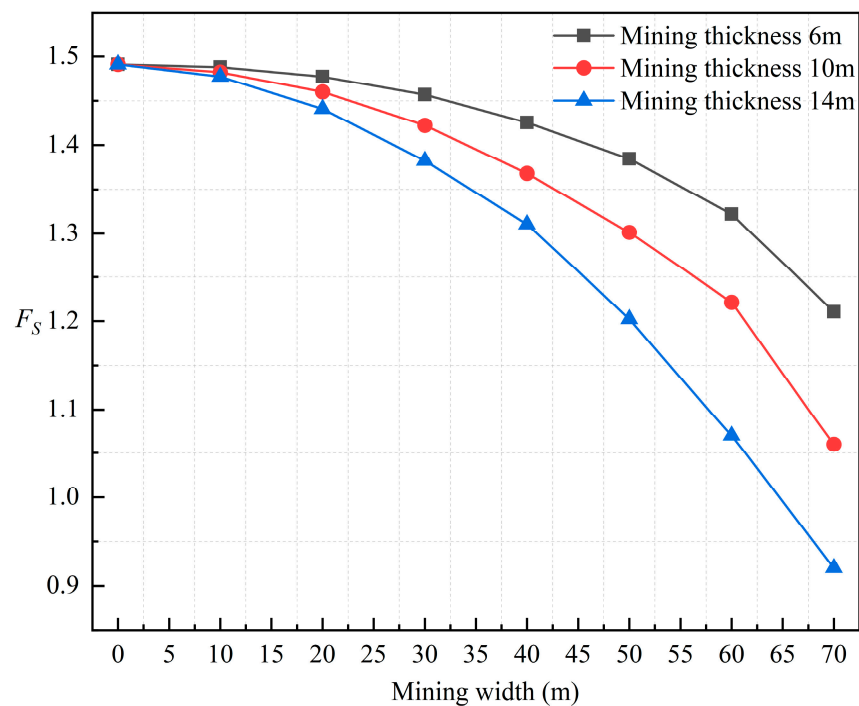


Figure 17. Slope safety factor under different mining thicknesses.

5.2. The Influence of Mining Direction

To analyze the influence of the mining direction on the stability of the slope, we continue to use the model from case study 2. The 4# coal seam is excavated in different directions from the same starting position, which is directly below the middle of the slope. For every 10 m of excavation, the IRMO algorithm with Lévy flight is used to calculate the safety factor F_S of the clay slope after excavation. Table 12 shows the parameter settings of different mining directions.

Table 12. Parameter settings of mining direction.

Mining Direction	Mining Thickness $M/(m)$	Mining Depth $H/(m)$	The x-Coordinate of the Excavation Starting Position (m)	The Length of Each Step of Excavation (m)
Mining along the slope	10	74	250	10
Mining against the slope	10	74	250	10

From Figure 18, it can be observed that when the excavation starting position is below the middle position of the slope, the safety factor F_S of mining along the slope is always greater than that of mining against the slope, and the difference in the safety factor gradually increases with the increase in the mining width. When mining along the slope, F_S reaches 1.2211 at the mining width of 60 m, close to the critical safety factor of 1.2 specified in the regulations. However, when mining against the slope, F_S decreases to 1.2103 at the mining width of 50 m, already reaching the critical safety factor specified in the regulations. Continuing excavation to 70 m results in an F_S of only 0.91, indicating a significant risk of instability.

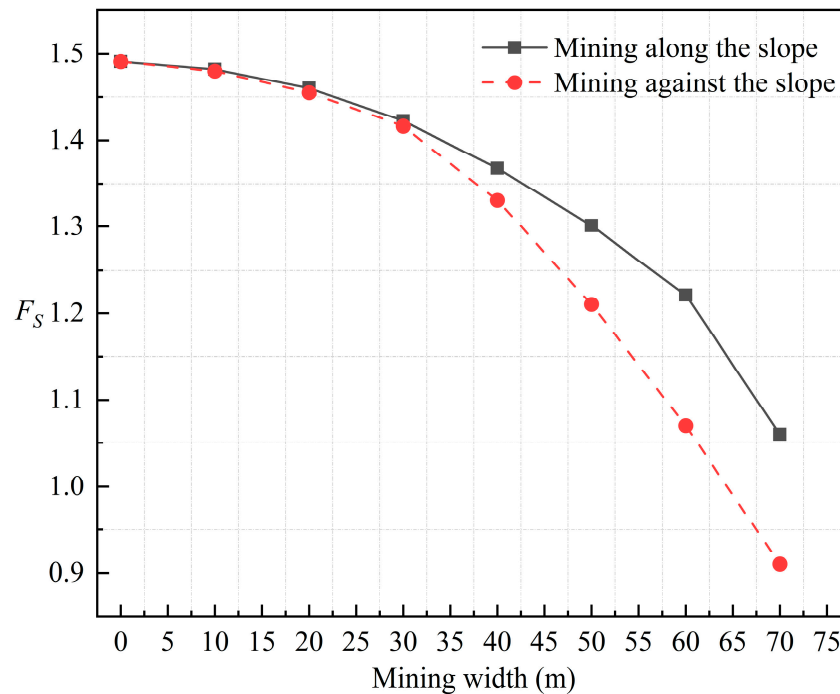


Figure 18. Slope safety factor under different mining directions.

6. Discussion

This study proposes a new method for analyzing the stability of soil slopes under underground coal mining based on the IRMO algorithm with Lévy flight, which can quickly and accurately evaluate the stability of slopes under the influence of coal seam mining. This method can be used as a supplement to the mine slope safety warning system and integrated with existing mining systems. By inputting parameters such as the soil material properties of the slope, coal mining conditions, the subsidence and deformation of the slope, and the parameters of the IRMO algorithm with Lévy flight, the safety factor of the slope can be calculated to evaluate its stability. In the implementation process, the parameter data play a decisive role in the accuracy of the results. If the data of the parameters used differ significantly from the actual situation, the calculated results will lose their reference significance. Therefore, the issue of data synchronization in the mining system deserves attention. For example, the subsidence and deformation of the slope after coal mining is a long-term process, and the data from the mining area displacement monitoring system need to be updated promptly to ensure the accuracy of the data. The data on coal mining

conditions are associated with the complexity of geological conditions and the management, scheduling, and maintenance of mining equipment, which may result in discrepancies between the planned mining thickness and depth and the actual mining thickness and depth at different mining locations. Therefore, timely data synchronization is necessary.

The method proposed in this study can also provide references for optimizing mining operations. By calculating the safety factor of slopes under different mining thicknesses and mining directions in case study 2, the variation in the safety factor of slopes under different mining conditions is studied. Smaller mining thicknesses result in higher safety factors for slopes under the same mining width, which is more conducive to slope stability. When the excavation starting position is below the middle position of the slope, the mining direction of mining along the slope is more favorable for slope stability. Furthermore, after determining the mining thickness and mining direction, this method can also be used to determine the maximum allowable mining width of the coal seam, which corresponds to the mining width when the safety factor of the slope reaches the critical safety factor specified in the regulation.

On the other hand, this study still has certain limitations and shortcomings. For instance, when selecting parameters, it did not consider factors such as the skill level of workers and the communication and collaboration capabilities of the mining team, thus overlooking the impact of human factors on slope stability [36]. Additionally, this study did not account for the influence of rainfall. Rainfall infiltration can change the matric suction of soil, reduce the soil shear strength, and significantly decrease slope stability [37]. Analyzing the stability of mining slopes under rainfall conditions can help prevent slope instability and ensure the safety of mining areas [38]. Therefore, further research is needed to address these aspects.

7. Conclusions

This study considered the impact of underground coal seam mining and conducted a limit equilibrium analysis of the slope based on the rigorous Janbu method, and the IRMO algorithm with Lévy flight was used to conduct global optimization to obtain the critical sliding surface and the corresponding minimum safety factor of soil slopes under underground coal mining conditions. The stability issues of soil slopes under underground coal seam mining are investigated. The details are as follows:

1. The simulation results of the benchmark functions show that combining the IRMO algorithm and Lévy flight can significantly enhance the performance of solving non-linear multi-dimensional optimization problems, preventing it from getting trapped in local optima.
2. Through an analysis of three different case studies involving slope under full mining, slope under stepwise mining, and the sliding fissures of slope, the feasibility of applying the IRMO algorithm with Lévy flight to a stability analysis of soil slopes under underground coal seam mining is demonstrated. The algorithm exhibits excellent performance in computing the convergence efficiency and ensuring the accuracy and stability of the results.
3. By calculating the safety factors of soil slopes under different mining thicknesses and mining directions, it was evident that both factors have a significant impact on the stability of slopes. Smaller mining thicknesses result in a higher safety factor for slopes under the same mining width, which is more favorable for slope stability. And mining along the slope is more advantageous for slope stability compared to mining against the slope when the excavation starting position is below the middle position of the slope. In addition, when the safety factor of the slope decreases to the critical safety factor specified in the regulation, continuing excavation will significantly reduce the stability of the slope.

Author Contributions: Conceptualization, L.J. and H.L.; methodology, H.L.; software, H.L.; validation, H.L.; formal analysis, H.L.; investigation, H.L.; resources, H.L.; data curation, H.L.; writing—original draft preparation, H.L.; writing—review and editing, L.J.; visualization, P.L.; supervision, L.J.; project administration, L.J. All authors have read and agreed to the published version of the manuscript.

Funding: This research received no external funding.

Data Availability Statement: The data supporting the conclusions of this article will be made available by the authors upon request.

Conflicts of Interest: The authors declare no conflicts of interest.

References

1. Yang, C.; Shi, W.; Qian, X.; Peng, X. Deformation and Failure Mechanism of Bedding Slopes Induced by Underground Mining: Case Study from Yanwan Village, Guizhou Province, China. *Geotech. Geol. Eng.* **2023**, *41*, 1877–1891. [[CrossRef](#)]
2. Li, S.; Zhao, Z.; Hu, B.; Yin, T.; Chen, G.; Chen, G. Hazard Classification and Stability Analysis of High and Steep Slopes from Underground to Open-Pit Mining. *Int. J. Environ. Res. Public Health* **2022**, *19*, 11679. [[CrossRef](#)]
3. Lian, X.; Hu, H.; Li, T.; Hu, D. Main Geological and Mining Factors Affecting Ground Cracks Induced by Underground Coal Mining in Shanxi Province, China. *Int. J. Coal Sci. Technol.* **2020**, *7*, 362–370. [[CrossRef](#)]
4. Liu, N.; Zhao, X.-G.; Song, S.-J.; Zhou, W.-F. Effect of Underground Coal Mining on Slope Morphology and Soil Erosion. *Math. Probl. Eng.* **2019**, *2019*, 5285126. [[CrossRef](#)]
5. Han, C.; Zu, F.; Du, C.; Shi, L. Analysis of Excavation Stability and Reinforcement Treatment of the Cutting Slope under the Influence of Old Goaf. *Appl. Sci.* **2022**, *12*, 8698. [[CrossRef](#)]
6. Sun, X.; Ho, C.-H.; Li, C.; Xia, Y.; Zhang, Q. Inclination Effect of Coal Mine Strata on the Stability of Loess Land Slope under the Condition of Underground Mining. *Nat. Hazards* **2020**, *104*, 833–852. [[CrossRef](#)]
7. Wang, W.; Li, J.; Wang, C.; Chen, S.; Wang, P. Analysis of failure mode and deformation evolution characteristics of slopes under the influence of highwall mining. *Coal Sci. Technol.* **2023**, *51*, 321–336. [[CrossRef](#)]
8. Ding, Q.-L.; Peng, Y.-Y.; Cheng, Z.; Wang, P. Numerical Simulation of Slope Stability during Underground Excavation Using the Lagrange Element Strength Reduction Method. *Minerals* **2022**, *12*, 1054. [[CrossRef](#)]
9. Shi, S.; Guo, Z.; Ding, P.; Tao, Y.; Mao, H.; Jiao, Z. Failure Mechanism and Stability Control Technology of Slope during Open-Pit Combing Underground Extraction: A Case Study from Shanxi Province of China. *Sustainability* **2022**, *14*, 8939. [[CrossRef](#)]
10. Vanneschi, C.; Eyre, M.; Burda, J.; Žižka, L.; Francioni, M.; Coggan, J.S. Investigation of Landslide Failure Mechanisms Adjacent to Lignite Mining Operations in North Bohemia (Czech Republic) through a Limit Equilibrium/Finite Element Modelling Approach. *Geomorphology* **2018**, *320*, 142–153. [[CrossRef](#)]
11. Li, S.; Zhao, Z.; Hu, B.; Yin, T.; Chen, G.; Chen, G. Three-Dimensional Simulation Stability Analysis of Slopes from Underground to Open-Pit Mining. *Minerals* **2023**, *13*, 402. [[CrossRef](#)]
12. Leng, D.; Shi, W.; Liang, F.; Li, H.; Yan, L. Stability and Deformation Evolution Analysis of Karstified Slope Subjected to Underground Mining Based on Hoek–Brown Failure Criterion. *Bull. Eng. Geol. Environ.* **2023**, *82*, 174. [[CrossRef](#)]
13. Zhang, Z.; Ma, N.; Liang, X.; Wang, L. Analysis of influence factors of goaf on slope stability. *Coal Technol.* **2019**, *38*, 94–96. [[CrossRef](#)]
14. Xu, T.; Yin, Z.; Deng, Y. Stability Analysis of Bedding Rock Slope at Underground Mining Conditions. *Chin. J. Undergr. Space Eng.* **2011**, *7*, 1241–1245+1262.
15. Shi, L.; Li, X.; Sun, G.; Bai, B. Research on stability of open-mining slope under underground mining. *Rock Soil Mech.* **2012**, *33*, 812–820. [[CrossRef](#)]
16. Zhang, Y.; Tang, J.; Li, G.; Teng, J. Influence of Depth-Thickness Ratio of Mining on the Stability of a Bedding Slope with Its Sliding Surface in Concave Deformation. *Int. J. Min. Sci. Technol.* **2016**, *26*, 1117–1123. [[CrossRef](#)]
17. Yang, Y.; Zhou, W.; Jiskani, I.M.; Lu, X.; Wang, Z.; Luan, B. Slope Stability Prediction Method Based on Intelligent Optimization and Machine Learning Algorithms. *Sustainability* **2023**, *15*, 1169. [[CrossRef](#)]
18. Zolfaghari, A.R.; Heath, A.C.; McCombie, P.F. Simple Genetic Algorithm Search for Critical Non-Circular Failure Surface in Slope Stability Analysis. *Comput. Geotech.* **2005**, *32*, 139–152. [[CrossRef](#)]
19. Yang, Y.; Wu, W.; Zhang, J.; Zheng, H.; Xu, D. Determination of Critical Slip Surface and Safety Factor of Slope Using the Vector Sum Numerical Manifold Method and MAX-MIN Ant Colony Optimization Algorithm. *Eng. Anal. Bound. Elem.* **2021**, *127*, 64–74. [[CrossRef](#)]
20. Gandomi, A.H.; Kashani, A.R.; Mousavi, M.; Jalalvandi, M. Slope Stability Analyzing Using Recent Swarm Intelligence Techniques. *Num. Anal. Meth. Geomech.* **2015**, *39*, 295–309. [[CrossRef](#)]
21. Himanshu, N.; Burman, A.; Kumar, V. Numerical Study of Optimal Location of Non-Circular Segmented Failure Surface in Soil Slope with Weak Soil Layer. *Int. J. Appl. Metaheuristic Comput.* **2021**, *12*, 111–141. [[CrossRef](#)]
22. Jin, L.; Feng, Q. Improved Radial Movement Optimization to Determine the Critical Failure Surface for Slope Stability Analysis. *Environ. Earth Sci.* **2018**, *77*, 564. [[CrossRef](#)]

23. Jin, L.; Wei, J.; Luo, C.; Qin, T. Slope Stability Analysis Based on Improved Radial Movement Optimization Considering Seepage Effect. *Alex. Eng. J.* **2023**, *79*, 591–607. [[CrossRef](#)]
24. Pan, Z.; Jin, L.; Chen, W. Improved radial movement optimization algorithm for slope stability analysis. *Rock Soil Mech.* **2016**, *37*, 2079–2084. [[CrossRef](#)]
25. Jin, L.; Qin, T.; Liu, P. Upper Bound Solution Analysis of the Ultimate Bearing Capacity of Two-Layered Strip Foundation Based on Improved Radial Movement Optimization. *Appl. Sci.* **2023**, *13*, 7299. [[CrossRef](#)]
26. Ling, Y.; Zhou, Y.; Luo, Q. Lévy Flight Trajectory-Based Whale Optimization Algorithm for Global Optimization. *IEEE Access* **2017**, *5*, 6168–6186. [[CrossRef](#)]
27. Michalowski, R.L. Stability Assessment of Slopes with Cracks Using Limit Analysis. *Can. Geotech. J.* **2013**, *50*, 1011–1021. [[CrossRef](#)]
28. Liu, H.; Deng, K.; Lei, S.; Bian, Z. Mechanism of Formation of Sliding Ground Fissure in Loess Hilly Areas Caused by Underground Mining. *Int. J. Min. Sci. Technol.* **2015**, *25*, 553–558. [[CrossRef](#)]
29. He, W. *Mining Subsidence and Damage in Mountains Region*; Chinese Science and Technology Press: Beijing, China, 2003.
30. Rahmani, R.; Yusof, R. A New Simple, Fast and Efficient Algorithm for Global Optimization over Continuous Search-Space Problems: Radial Movement Optimization. *Appl. Math. Comput.* **2014**, *248*, 287–300. [[CrossRef](#)]
31. Jensi, R.; Jiji, G.W. An Enhanced Particle Swarm Optimization with Levy Flight for Global Optimization. *Appl. Soft Comput.* **2016**, *43*, 248–261. [[CrossRef](#)]
32. Mantegna, R.N. Fast, Accurate Algorithm for Numerical Simulation of Lévy Stable Stochastic Processes. *Phys. Rev. E* **1994**, *49*, 4677–4683. [[CrossRef](#)] [[PubMed](#)]
33. Zhao, B.; Guo, Y.; Wang, W.; He, S. Impact of Underground Coal Seam Mining on Stability and Slippage of the Loess Slope. *Sustainability* **2023**, *15*, 6485. [[CrossRef](#)]
34. Ren, P. Study on Deformation and Instability Mechanism of Red Clay Slope under the Influence of Goaf. Ph.D. Thesis, China Coal Research Institute, Beijing, China, 2020. [[CrossRef](#)]
35. *GB 50197-2015*; Design Code for Open-Pit Mine in Coal Industry. China Planning Publishing House: Beijing, China, 2015.
36. Li, Y.; Wu, X.; Luo, X.; Gao, J.; Yin, W. Impact of Safety Attitude on the Safety Behavior of Coal Miners in China. *Sustainability* **2019**, *11*, 6382. [[CrossRef](#)]
37. Theocharis, A.I.; Zevgolis, I.E.; Deliveris, A.V.; Karametou, R.; Koukouzas, N.C. From Climate Conditions to the Numerical Slope Stability Analysis of Surface Coal Mines. *Appl. Sci.* **2022**, *12*, 1538. [[CrossRef](#)]
38. Li, X.; Qin, Z.; Tian, Y.; Zhang, H.; Zhao, H.; Shen, J.; Shao, W.; Jiang, G.; Guo, X.; Zhang, J. Study on Stability and Ecological Restoration of Soil-Covered Rocky Slope of an Abandoned Mine on an Island in Rainy Regions. *Sustainability* **2022**, *14*, 12959. [[CrossRef](#)]

Disclaimer/Publisher’s Note: The statements, opinions and data contained in all publications are solely those of the individual author(s) and contributor(s) and not of MDPI and/or the editor(s). MDPI and/or the editor(s) disclaim responsibility for any injury to people or property resulting from any ideas, methods, instructions or products referred to in the content.